nanomaterials

MDPI

Article

Highly Efficient and Controllable Methodology of the $Cd_{0.25}Zn_{0.75}Se/ZnS$ Core/Shell Quantum Dots Synthesis

Liudmila Loghina [1,*], Maksym Chylii [1], Anastasia Kaderavkova [1], Stanislav Slang [1], Petr Svec [2], Jhonatan Rodriguez Pereira [1], Bozena Frumarova [1], Miroslav Cieslar [3] and Miroslav Vlcek [1]

[1] Center of Materials and Nanotechnologies, Faculty of Chemical Technology, University of Pardubice, 53002 Pardubice, Czech Republic; Maksym.Chylii@upce.cz (M.C.); Anastasia.Kaderavkova@upce.cz (A.K.); Stanislav.Slang@upce.cz (S.S.); Jhonatan.RodriguezPereira@upce.cz (J.R.P.); Bozena.Frumarova@upce.cz (B.F.); Miroslav.Vlcek@upce.cz (M.V.)

[2] Department of General and Inorganic Chemistry, Faculty of Chemical Technology, University of Pardubice, 53210 Pardubice, Czech Republic; petr.svec2@upce.cz

[3] Faculty of Mathematics and Physics, Charles University, 12116 Prague, Czech Republic; cieslar@met.mff.cuni.cz

* Correspondence: Liudmila.Loghina@upce.cz

Abstract: The surface of any binary or multi-component nanocrystal has imperfections and defects. The number of surface defects depends both on the nature of the nanomaterial and on the method of its preparation. One of the possibilities to confine the number of surface defects is the epitaxial growth of the shell, which leads to a change in the physical properties while maintaining the morphology of the core. To form a shell of the desired thickness, an accurate calculation of the amount of its precursors is substantial to avoid the appearance of individual crystals consisting of the shell material. This study aimed to develop an effective calculation method for the theoretical amount of precursors required for the formation of a ZnS shell on the surface of a $Cd_{0.25}Zn_{0.75}Se$ core, followed by the practical implementation of theoretical calculations and characterization of the prepared nanomaterials. This method allows the complete control of the masses and volumes of the initial reagents, which will in turn prevent undesirable nucleation of nuclei consisting of the shell material. In the synthesis of $Cd_{0.25}Zn_{0.75}Se/ZnS$ core/shell quantum dots (QDs), the sources of chalcogens were substituted seleno- and thioureas, which are capable of not only supplanting modern toxic sources of sulfur and selenium but also allowing one to perform the controlled synthesis of highly photoluminescent QDs with a low number of surface defects. The result of this shell overcoating method was an impetuous augmentation in the photoluminescence quantum yield (PL QY up to 83%), uniformity in size and shape, and a high yield of nanomaterials. The developed synthetic technique of core/shell QDs provides a controlled growth of the shell on the core surface, which makes it possible to transfer this method to an industrial scale.

Keywords: core/shell quantum dots; controllable synthesis; methodology; non-toxic chalcogen source

Citation: Loghina, L.; Chylii, M.; Kaderavkova, A.; Slang, S.; Svec, P.; Rodriguez Pereira, J.; Frumarova, B.; Cieslar, M.; Vlcek, M. Highly Efficient and Controllable Methodology of the $Cd_{0.25}Zn_{0.75}Se/ZnS$ Core/Shell Quantum Dots Synthesis. *Nanomaterials* **2021**, *11*, 2616. https://doi.org/10.3390/nano11102616

Academic Editor: Lavinia Balan

Received: 16 September 2021
Accepted: 30 September 2021
Published: 5 October 2021

1. Introduction

Over the past decades, ternary semiconductor quantum dots (QDs) have drawn vast scientific and technological interest due to their unique size-, shape-, composition-dependent physical, chemical, and optoelectronics properties [1–3]. The technological importance of such QDs (CdZnS, CdZnSe, CdSSe, etc.) is determined by the tunability of their emission and absorbance features, which opens up wide possibilities for applications in diverse fields such as light-emitting diodes (LEDs) [4], solar cells [5], alpha, gamma, and neutron scintillators [6–8], catalysts for reaction processes [9–11], and bio labeling [12]. In particular, CdZnSe QDs have attracted research focus because of the possibility to adjust the compositional Cd:Zn ratio and thus to tune the emission color over the whole visible spectrum [13,14]. Another successful synthetic strategy for the preparation of highly

photoluminescent Cd-Zn-Se QDs with PL QYs up to 64% by using (Z)-1-hexyl-3-(octadec-9-enyl)selenourea as a new selenium precursor was recently presented [15].

However, ternary semiconductor QDs suffer from poor stability against the surrounding environment due to the surface defects that act as nonradiative recombination sites [16,17]. Such a phenomenon leads to the degradation of PL QY and hinders the actual application of QDs. Growing a mono- or multilayer shell on the QD's core is one of the effective approaches to solve this problem. Usually, the outer shell is a wide-bandgap semiconductor material that provides effective elimination of surface-related defects in the core QDs, which leads to passivation of the surface, improved photostability, better dispersibility [18–21], suppressed Forster resonance energy transfer (FRET), and enhanced optical characteristics (PL QY, emission wavelength, and carrier lifetime) of QDs. These properties are essential for the future commercial applications of core/shell QDs. Recently, the research focus turned to the ternary core/shell systems with different shell compositions, such as CdSeS/ZnS [22,23], CdZnSe/ZnSe [24–26], CdTeSe/ZnSe [27,28], and CdZnS/ZnS [29,30] QDs. It is important to note that to achieve the desired optical characteristics and an increase in PL QY, careful selection of the appropriate composition of both core and shell QDs (considering their bandgap and lattice mismatch) and also the thickness of the shell is required. Until now, several strategies for the synthesis of core/shell ternary QDs have been reported. Fitzmorris et al. [31] introduced a synthetic approach that greatly enhanced the PL QY (from 9.6% for CdZnSe QDs core to 42% for $Cd_{1-x}Zn_xSe/ZnSe$ and 63% for $Cd_{1-x}Zn_xSe/ZnSe/ZnS$) of $Cd_{1-x}Zn_xSe/ZnSe/ZnS$ after a shell growth. The CdZnSe core was prepared at 320 °C/1 h in one step without any purification process using oleic acid and oleylamine as surface ligands; then, ZnSe and ZnS shells were formed by the successive injection of precursors (TOP-Se and TOP-S) in one-pot at 240 °C and 200 °C, respectively.

Later, Zhang et al. [32] prepared CdZnSe/ZnSe quantum dots via the modified one-pot method [31]. CdZnSe QDs were synthesized at 290–310 °C/8 min with oleic acid and without oleylamine. Then, the reaction mixture was heated to 300–320 °C and the Se-TBP precursor was slowly injected. By varying the reaction temperatures and Se-TBP amount (1–2.5 mmol) within the shell formation, the absolute PL QY increased from 20% to 50%.

Susumu et al. [33] reported a series of $Cd_xZn_{1-x}Se/Cd_yZn_{1-y}S/ZnS$ and $ZnSe/Cd_yZn_{1-y}S/ZnS$ QDs prepared from ZnSe cores (synthesized from diethylzinc and Se-TOP in oleylamine solution at 290 °C) with a subsequent surface modification by ligand exchange with hydrophilic compact ligands. $Cd_xZn_{1-x}Se$ cores were formed via cation exchange with Cd^{2+} ions from as-prepared ZnSe QDs in 1-octadecene (ODE), oleylamine, TOP, and dodecylphosphonic acid solution at 220 °C. Following that, overcoating with $Cd_yZn_{1-y}S$ and ZnS shells was conducted in the same flask by adding Zn and Cd oleate solutions and a ~1.2–1.5-fold excess of *n*-octanethiol (with respect to metal precursors) at 290–310 °C for 4–6 h. The PL QY of the prepared core/shell $Cd_xZn_{1-x}Se/Cd_yZn_{1-y}S/ZnS$ QDs enhanced from 1–2% after cation exchange to 53%.

Recently, Jin et al. [24] presented a cation exchange-assisted method for the preparation of ZnCdSe/ZnSe core/shell QDs. The typical synthesis was carried out by employing CdO, zinc acetate, oleic acid, and ODE at 300 °C with an injection of Se-TOP precursor. After 12 min of the reaction process, an additional amount of Se-TOP in ODE was dripped to the solution. The shell formation took 30 min. The resulting core/shell ZnCdSe/ZnSe (8 monolayers) QDs reached an absolute PL QY of 99%. In addition, the authors reported a detailed calculation for the amount of shell precursors required to form a different number of monolayers.

Despite the variety of proposed methods, it remains a challenging task to synthesize CdZnSe cores with an appropriate shell thickness and high PL QY using nontoxic sources of S and Se.

Herein, we successfully elaborated on an efficient way of shell growth on the already formed QDs core. The presented method is based on the calculated ratio of the volume/mass of the core to the shell. Gram-scale synthesis of the $Cd_{0.25}Zn_{0.75}Se$ core

(3.5 g) was carried out by a hot-injection method followed by the reaction with a calculated amount of cadmium and zinc linoleates with (*Z*)-*N*-(octadec-9-enyl)morpholine-4-carboselenoamide (*N*,*N*′,*N*′-trisubstituted selenourea), which was not previously used as a source of selenium. The shell, consisting of 1–5 monolayers (MLs) of zinc sulfide, grew on the core upon precisely dosed injection of a calculated amount of (*Z*)-1-(octadec-9-enyl)-3-phenylthiourea dissolved in a mixture of oleylamine and 1-octadecene at 240 °C, to a diluted solution of a half-fold excess of zinc linoleate and the core. The dosed injection of the sulfur source avoids the parallel formation of zinc sulfide cores and ensures uniform shell formation. The presented method for calculating the amount of materials, required for a shell growth of the desired thickness, makes possible the application of this technique to the synthesis of core/shell QDs of any composition and size. In our opinion, the availability of precursors, as well as the simplicity and reproducibility of calculations of the materials required to grow a shell of the desired thickness, makes the proposed gram-scale method promising for the widespread production of LEDs and bio-, light-, and chemical sensors.

2. Materials and Methods

2.1. Materials

Cadmium oxide (CdO, 99.99%), zinc oxide (ZnO, 99%), 1-octadecene (ODE, technical grade, 90%), linoleic acid (LA, technical grade 60–74%), oleylamine (OAm, technical grade, 90%), selenium (Se, 99.999%), phenyl isothiocyanate (PhNCS, 98%), morpholine (99%), chloroform-d ($CDCl_3$, 99.8 atom % D), and silica gel (high-purity grade, pore size 60 Å, 230–400 mesh particle size) were purchased from Sigma-Aldrich and used without further purification. Sodium hydroxide (NaOH, p.a.) and solvents were purchased from Fisher Scientific and used for the purification of organic precursors and QDs. Triethylamine (Et_3N, p.a.) and tetrahydrofuran (THF, p.a.) were purified by distillation over NaOH and sodium correspondingly prior to the synthesis. Syntheses of QDs were carried out using standard Schlenk techniques under an inert atmosphere.

2.2. Synthesis of Selenium and Sulphur Precursors

2.2.1. Synthesis of (Z)-1-isocyanooctadec-9-ene

Oleylamine (OAm, 0.01 mol) in 40 mL of CH_2Cl_2 and $CHCl_3$ (0.11 mol) were added to a freshly prepared 50% NaOH solution (22.80 g, 0.57 mol). After that, a phase transfer catalyst (tetraethylammonium bromide, 0.005 mol) was added to the resulting mixture mechanically stirred at room temperature. Afterward, the reaction mixture was stirred under reflux for 24 h. The synthesis was controlled by thin-layer chromatography (TLC) (CH_2Cl_2). The resulting reaction mixture was poured into 100 mL of water and then extracted with CH_2Cl_2 (3 × 50 mL). The combined organic extracts were washed with aqueous NH_4Cl (sat.), brine, and then dried over anhydrous Na_2SO_4. After the solvent evaporation, the residue was purified by flash chromatography (CH_2Cl_2). A colorless liquid was obtained in a 63% yield.

^{1}H NMR (500.13 MHz, $CDCl_3$), ppm: 5.27–5.37 (m, 2H, -CH=CH-), 3.34–3.36 (m, 2H, CH_2), 1.98–2.03 (m, 2H, CH_2), 1.62–1.69 (m, 2H, CH_2), 1.39–1.45 (m, 2H, CH_2), 1.25–1.30 (m, 22H, 11 × CH_2), 0.85–0.89 (t, 3H, CH_3).

^{13}C NMR (125.76 MHz, $CDCl_3$), ppm: 155.9 (N≡C), 130.0, (CH=CH), 129.7 (CH=CH), 41.50 (m, CH_2N≡C), 32.0, 29.8, 29.7, 29.6, 29.5, 29.4, 29.3, 29.2, 29.1, 28.7, 27.3, 27.2, 26.3, 22.7, 14.2.

2.2.2. Synthesis of (Z)-1-isoselenocyanatooctadec-9-ene

Dry Et_3N (0.026 mol) and (*Z*)-1-isocyanooctadec-9-ene (0.026 mol) in 50 mL of dry THF were mixed in a reaction flask. The mixture was degassed and selenium powder (0.013 mol) was added under Ar. The reaction mixture was heated to reflux for 8 h under Ar and then naturally cooled to room temperature. Afterward, the second portion of selenium was added (0.013 mol) and heated until the complete dissolution of selenium. The resulting

clear solution was concentrated, followed by purification on silica gel using petroleum ether as an eluent. A yellowish liquid product was obtained in 88% yield.

^{1}H NMR (500.13 MHz, $CDCl_3$), ppm: 5.27–5.35 (m, 2H, -CH = CH-), 3.57 (t, 2H, *J* = 6.7 Hz, -CH_2-NCSe), 1.93–1.99 (m, 2H, CH_2), 1.67–1.73 (m, 2H, CH_2), 1.36–1.42 (m, 2H, CH_2), 1.23–1.28 (m, 22H, 11 × CH_2), 0.85 (t, 3H, *J* = 6.7 Hz, CH_3).

^{13}C NMR (125.76 MHz, $CDCl_3$), ppm: 130.0 (CH = CH), 129.7 (CH = CH), 122.0 (N = C = Se), 45.5 (br, CH_2NCSe), 32.4 (m), 29.9, 29.7, 29.6, 29.5, 29.4, 29.3, 29.2, 29.0, 28.8, 27.3, 27.2, 26.5, 22.7, 14.2. ^{77}Se NMR (95.35 MHz, $CDCl_3$), ppm: −358.3.

2.2.3. Synthesis of (*Z*)-*N*-(octadec-9-enyl)morpholine-4-carboselenoamide

To a solution of (*Z*)-1-isoselenocyanatooctadec-9-ene (0.02 mol) in 100 mL of CH_2Cl_2, morpholine (0.02 mol) was added. The reaction mixture was stirred for 1 h without any exposure to light. The reaction was monitored by TLC (CH_2Cl_2). After the solvent evaporation, a light-yellow semisolid was collected. The reaction yield was quantitative.

^{1}H NMR (500.13 MHz, $CDCl_3$), ppm: 6.06 (br, 1H, NH), 5.26–5.32 (m, 2H, -CH = CH-), 3.81 (s, 4H, 2 × CH_2), 3.64 (s, 6H, 3 × CH_2), 1.87–1.96 (m, 2H, CH_2), 1.52–1.61 (m, 4H, 2 × CH_2), 1.16–1.26 (m, 22H, 11 × CH_2), 0.79 (t, 3H, *J* = 6.84 Hz, CH_3).

^{13}C NMR (125.76 MHz, $CDCl_3$), ppm: 181.9 (C = Se), 129.6 (2xCH = CH), 66.0, 49.2, 48.9, 31.7, 29.6, 29.4, 29.2, 29.1, 27.1, 26.8, 22.6, 14.0.

2.2.4. Synthesis (Z)-1-(octadec-9-enyl)-3-phenylthiourea

To a solution of phenyl isothiocyanate (0.05 mol) in CH_2Cl_2 (75 mL), oleylamine (0.05 mol) was added dropwise with permanent stirring at room temperature (exothermic process). The reaction was stirred for one hour under the monitoring by TLC (CH_2Cl_2). After distilling off the solvent, the semisolid was obtained with quantitative yield.

^{1}H NMR (500.13 MHz, $CDCl_3$), ppm: 8.42 (br, 1H, NH), 7.40 (t, 2H, *J* = 7.8 Hz, Ph), 7.25–7.28 (m, 1H, Ph), 7.19–7.21 (d, 2H, *J* = 7.8 Hz, Ph), 6.08 (br, 1H, NH), 5.31–5.37 (m, 2H, -CH = CH-), 3.57–3.61 (m, 2H, CH_2), 1.93–2.01 (m, 2H, CH_2), 1.51–1.57 (m, 2H, CH_2), 1.23–1.31 (m, 22H, 11 × CH_2), 0.86 (t, 3H, *J* = 6.9 Hz, CH_3).

^{13}C NMR (125.76 MHz, $CDCl_3$), ppm: 180.5 (C = S), 136.5 (Ph), 130.2 (Ph), 130.1 (CH = CH), 129.9 (CH = CH), 127.2 (Ph), 125.3 (Ph), 45.6 (CH_2NH), 32.0, 29.9, 29.8, 29.7, 29.6, 29.5, 29.4, 29.3, 29.2, 29.1, 27.3, 27.2, 27.0, 22.8, 14.2.

2.3. Preparation of $Cd_{0.25}Zn_{0.75}Se$/ZnS (1–5 MLs) QDs

2.3.1. Synthesis of Core $Cd_{0.25}Zn_{0.75}Se$

The reaction mixture consisting of CdO (0.005 mol), ZnO (0.015 mol), LA (0.06 mol), and 60 mL of ODE was degassed for 15–20 min at room temperature and then at 150 °C until complete homogenization. The temperature of the reaction mixture was then raised to 240 °C (the growth temperature) and a solution of (*Z*)-N-(octadec-9-enyl)morpholine-4-carboselenoamide (*SU*, 0.019 mol) in 9.4 mL of OAm and 1.6 mL of ODE was injected in one portion. All steps of the reaction process were carried out under vigorous stirring in an inert atmosphere. After the injection of the selenium precursor, the reaction mixture was further stirred for an additional 30 min while maintaining the growth temperature. The naturally cooled (40–45 °C) reaction mixture was diluted twofold with $CHCl_3$, and QDs were precipitated using a mixture of acetone and methanol (20:1). The formed precipitate was separated by centrifugation (10.000 rpm, 7 min). The separated QDs were dissolved in a minimum amount of $CHCl_3$ followed by precipitation with acetone. This procedure was carried out 3 more times to remove the starting components and solvent. The purified QDs were dried under vacuum for 5 h. The yield of core $Cd_{0.25}Zn_{0.75}Se$ was 3.5 g.

To determine the amount of $Cd_{0.25}Zn_{0.75}Se$ substance with a known mass of QDs stabilized by an organic shell, the chemical decomposition of the nanomaterial was carried out. Dried to the constant weight, $Cd_{0.25}Zn_{0.75}Se$ QDs (0.200 g) were added in 10% HCl (20 mL) and stirred at room temperature for 3 h. The organic layer was extracted with diethyl ether (3 × 20 mL). The combined organic extracts were washed with brine and

dried over Na_2SO_4. The ether extract was quantitatively filtered through a thin layer of silica gel. The mass of the residue obtained after distilling off the solvent was 0.031 g. Based on the performed procedure, it was found that 0.200 g of the nanomaterial contained 0.169 g of $Cd_{0.25}Zn_{0.75}Se$.

2.3.2. Synthesis of Core/Shell $Cd_{0.25}Zn_{0.75}Se$/ZnS 1 ML QDs

The calculated amount of ZnO (0.00126 mol) was mixed with LA (1.57 mL) and ODE (4 mL) in a 50 mL Schlenk flask. The reaction mixture was degassed for 15–20 min at room temperature and then at 150 °C until complete homogenization. Then, the temperature was raised to 240 °C (the growth temperature) and the solution of $Cd_{0.25}Zn_{0.75}Se$ QDs (0.196) in 2 mL of ODE was added by one portion. The calculated amount of (*Z*)-1-(octadec-9-enyl)-3-phenylthiourea (*TU*, 0.000615 mol) was dissolved in ODE (1.25 mL) and OAm (0.5 mL). This solution was added in portions (0.2 mL/2 min) under vigorous stirring (inert atmosphere) to the resulting mixture of Zn linoleate with the core and following stirring for 10 min at 240 °C. Isolation and purification of core/shell QDs were performed similarly to the procedure described in the synthesis of $Cd_{0.25}Zn_{0.75}Se$ QDs. The weight of $Cd_{0.25}Zn_{0.75}Se$/ZnS 1 ML QDs after drying was 0.32 g.

2.3.3. Synthesis of Core/Shell $Cd_{0.25}Zn_{0.75}Se$/ZnS 2 ML QDs

The procedure was similar to the previous synthesis. For 0.196 g of core $Cd_{0.25}Zn_{0.75}Se$, ZnO (0.00278 mol), LA (3.46 mL), ODE (7 mL), and a solution of (*Z*)-1-(octadec-9-enyl)-3-phenylthiourea (0.00139 mol) in OAm (0.6 mL) and ODE (0.8 mL) were taken. The weight of $Cd_{0.25}Zn_{0.75}Se$/ZnS 2 ML QDs after drying was 0.43 g.

2.3.4. Synthesis of Core/Shell $Cd_{0.25}Zn_{0.75}Se$/ZnS 3 ML QDs

For 0.196 g of core $Cd_{0.25}Zn_{0.75}Se$, ZnO (0.00474 mol), LA (4.4 mL), ODE (9 mL), and a solution of (*Z*)-1-(octadec-9-enyl)-3-phenylthiourea (0.00237 mol) in OAm (1.0 mL) and ODE (1.0 mL) were taken. This solution was added in portions (0.3 mL/2 min). The weight of $Cd_{0.25}Zn_{0.75}Se$/ZnS 3 ML QDs after drying was 0.67 g.

2.3.5. Synthesis of Core/Shell $Cd_{0.25}Zn_{0.75}Se$/ZnS 4 ML QDs

For 0.196 g of core $Cd_{0.25}Zn_{0.75}Se$, ZnO (0.00712 mol), LA (6.6 mL), ODE (14 mL), and a solution of (*Z*)-1-(octadec-9-enyl)-3-phenylthiourea (0.00356 mol) in OAm (1.0 mL) and ODE (0.5 mL) were taken. This solution was added in portions (0.3 mL/2 min). The weight of $Cd_{0.25}Zn_{0.75}Se$/ZnS 4 ML QDs after drying was 0.79 g.

2.3.6. Synthesis of Core/Shell $Cd_{0.25}Zn_{0.75}Se$/ZnS 5 ML QDs

For 0.196 g of core $Cd_{0.25}Zn_{0.75}Se$, ZnO (0.00992 mol), LA (9.3 mL), ODE (20 mL), and a solution of (*Z*)-1-(octadec-9-enyl)-3-phenylthiourea (0.00496 mol) in OAm (2.0 mL) were taken. This solution was added in portions (0.4 mL/2 min). The weight of $Cd_{0.25}Zn_{0.75}Se$/ZnS 5 ML QDs after drying was 0.94 g.

2.4. Characterization

IR spectra in the region 50–450 cm^{-1} (resolution 2 cm^{-1}) were recorded on a Vertex 70v FT-IR spectrometer (Bruker, Germany) using a single-bounce diamond ATR crystal. The room-temperature Raman spectra were measured by the Raman spectrophotometer MultiRam (Bruker, Germany). The YAG:Nd laser line (1064 nm) was used for excitation. X-ray diffraction patterns (XRD) were registered using the PANalytical EMPYREAN powder X-Ray diffractometer (ALMELO, Netherlands) with Cu-Kα radiation (λ = 1.5418 Å). Data were obtained across a 2θ range of 20–70° with a step size of 0.05°.

The Nuclear Magnetic Resonance (NMR) spectra were recorded from solutions in $CDCl_3$ at 295 K on a Bruker Ascend^{TM} 500 spectrometer (equipped with Z-gradient 5 mm Prodigy cryoprobe) at frequencies of 500.13 MHz for ^1H, 125.76 MHz for $^{13}C\{^1H\}$, and 95.35 MHz for $^{77}Se\{^1H\}$. The solutions were obtained by dissolving approximately

20–40 mg of each compound in 0.6 mL of the deuterated solvent. The values of ^{1}H chemical shifts were calibrated to residual signals of $CDCl_3$ ($\delta(^{1}H)$ = 7.26 ppm). The values of ^{13}C chemical shifts are referred to signals of $CDCl_3$ ($\delta(^{13}C)$ = 77.23 ppm). The values of ^{77}Se chemical shifts are referred to Me_2Se ($\delta(^{77}Se)$ = 0.0 pm). Positive chemical shift values denote shifts to the higher frequencies relative to the standards.

The surface chemical composition was determined by X-ray photoelectron spectroscopy (XPS, ESCA 2SR, Scienta-Omicron) using a monochromatic Al Kα source (1486.6 eV). QDs were pressed into C tape for the XPS analysis, and the possible charging effects were compensated using an electron flood gun. The following sequence of spectra was recorded: survey, C *1s*, O *1s*, Cd *3d*, Zn *2p*, Se *3d*, S *2p*, and C *1s* again to verify the stability of the charge compensation as a function of time. The survey spectra were recorded at a pass energy of 150 eV, while the high-resolution spectra were recorded at a pass energy of 20 eV. The binding energy scale was referenced to adventitious carbon (284.8 eV) and the quantitative analysis was performed using sensitivity factors provided by the manufacturer.

$Cd_{0.25}Zn_{0.75}Se$ (core) and $Cd_{0.25}Zn_{0.75}Se$/ZnS 1–5 ML (core/shell) QDs were predeposited onto lacey-carbon-coated (with/without graphene oxide layer) copper grids, and TEM, STEM, HRTEM, and EDS analyses and mapping were performed using a JEOL 2200FS transmission electron microscope (JEOL, Japan) equipped with a Centurio SDD-EDS detector. The TEM samples of QDs were prepared by dropping of QDs solution on a TEM copper grid with ~1 nm-thick graphene oxide on a lacey carbon membrane. To visualize the structure of the QDs with sufficient atomic resolution and contrast, high-resolution TEM imaging (HRTEM) was performed. The chemical composition of the single QD was carried out in a form of elemental maps using energy-dispersive X-ray (EDS) microanalysis in high-angle annular dark-field (HAADF) STEM mode using a Centurio EDS. In addition, energy-dispersive X-ray microanalysis of bulk nanoparticles samples (EDS) was carried out using the scanning electron microscope LYRA 3 (Tescan, Czech Republic) equipped with the EDS analyzer Aztec X-Max 20 (Oxford Instruments) at an acceleration voltage of 20 kV and with an FEI SUPER-X 4-quadrant windowless detector with a 120 mm^2 total detection area and 0.7 sr solid angle. The sample was deposited onto a 3 nm carbon membrane copper grid.

The QDs optical properties were measured using a Fluorometer PTI QuantaMaster 400 (Horiba Scientific) to obtain PL data in the spectral range of 300–750 nm using an excitation wavelength of λ = 300–500 nm and UV-3600 (Shimadzu) spectrometer to obtain UV-VIS absorbance spectra in the spectral range of 200–700 nm. The PL lifetime measurements were performed using TCSPC accessories for a Fluorometer PTI QuantaMaster 400 with 362, 395, and 455 nm light pulse excitations and a pulse half-width of 0.8 ns produced by NanoLED-360, 375, and 455, respectively (Horiba Scientific). Photoluminescence decay kinetics curves were analyzed by PTI Felix GX software.

3. Results and Discussion

3.1. Synthesis of Core/Shell $Cd_{0.25}Zn_{0.75}Se$/ZnS (1–5 MLs) QDs

The application of di- and trisubstituted thio- and selenoureas as effective, available, and environmentally safe sources of chalcogens has been presented previously [15,34–36]. The syntheses of (*Z*)-*N*-(octadec-9-enyl)morpholine-4-carboselenoamide and (*Z*)-1-(octadec-9-enyl)-3-phenylthiourea (Figure 1) proceeded without any complications and with good yield, which can only be limited by the purity of the reagents.

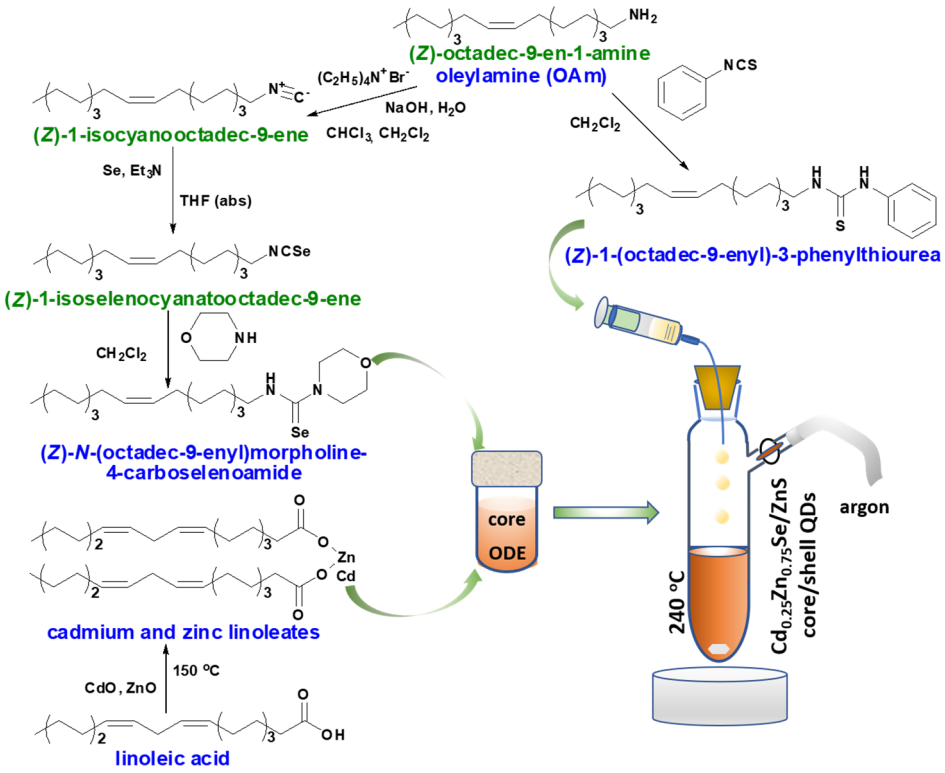

Figure 1. Schematic overview of the $Cd_{0.25}Zn_{0.75}Se/ZnS$ (1–5 MLs) core/shell QDs synthesis.

It was demonstrated that the formation of nanosized binary [35] and ternary sulfides [36] and selenides [15] begins with the formation of intermediate complexes of metal linoleates with substituted thio- or selenourea. The formed complex is unstable at high temperatures, which leads to its decomposition and initiates the onset of nucleation. Continuously forming nuclei grow by consuming the building material from the reaction medium. In parallel, the dissolution of smaller nuclei takes place, causing the homogeneity of the nanocrystals at the end of the reaction process. We presume that the creation of a shell on already formed and homogeneous nuclei occurs by a similar mechanism. To prevent the formation of nanocrystals grown from the shell material (i.e., ZnS), it is necessary to correlate the amounts of substances of all participants in the process. To determine the amount of the $Cd_{0.25}Zn_{0.75}Se$ substance, the resulting nanomaterial was chemically decomposed, namely, the selenide ion was replaced by chloride. When $Cd_{0.25}Zn_{0.75}Se$ QDs dried to constant weight were treated with 10% HCl, water-soluble metal chlorides and water-insoluble linoleic acid formed. During the further extraction, linoleic acid was fully transferred into diethyl ether. Thus, it was found that 0.196 g of nanomaterial contained 0.17 g of $Cd_{0.25}Zn_{0.75}Se$ QDs.

To develop a calculation model, we proceeded from empirical data, such as the average diameter (4.54 nm according to the TEM data, see Figure 2b) and the real composition of the synthesized spherical $Cd_{0.25}Zn_{0.75}Se$ core, and also from theoretical assumptions, such as the thickness of ZnS 1 ML, which is 0.31 nm for a cubic structure [37]. Thus, taking the shell radius (r_1) as a constant value, we can calculate the volume of the $Cd_{0.25}Zn_{0.75}Se$ core (V_1) and its mass (m_1), taking the density as a sum of the parts of the densities of binary selenides $\rho_{core} = 5.4 \times 10^6$ g/m^3 (Equations (1) and (2)):

$$V_1 = \frac{4}{3}\pi {r_1}^3 = 48.97 \text{ nm}^3 = 48.97 \cdot 10^{-27} \text{ m}^3 \quad (1)$$

$$m_1 = 5.4 \cdot 10^6 \cdot 48.97 \cdot 10^{-27} = 2.64 \cdot 10^{-19} \text{ g} \quad (2)$$

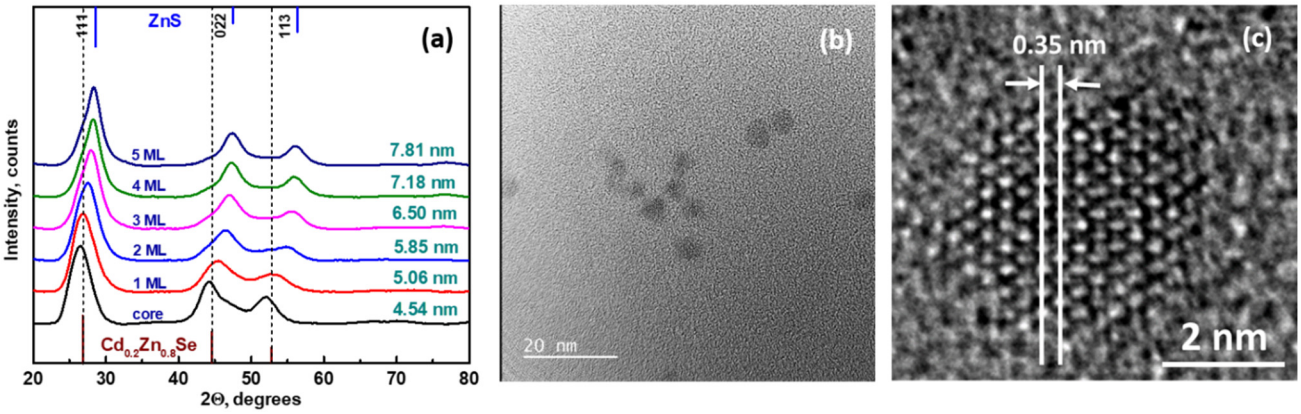

Figure 2. XRD patterns of $Cd_{0.25}Zn_{0.75}Se/ZnS$ QDs with different shell thicknesses (**a**), TEM (**b**), and HRTEM (**c**) images of $Cd_{0.25}Zn_{0.75}Se$ (core).

Therefore, if $r_2 = 0.31x + r_1$, where x is the number of monolayers, then at $x = 1$, m (ZnS 1 ML) will be 0.93×10^{-19} g (Equation (3)):

$$m_{shell} = V_{shell} \cdot \rho_{ZnS} = (V - V_1) \cdot 4.09 \cdot 10^6 = 0.93 \cdot 10^{-19} \text{ g} \quad (3)$$

where V is the volume of the $Cd_{0.25}Zn_{0.75}Se/ZnS$ core/shell and ρ_{ZnS} is the density of ZnS.

Taking the mass of the core as 100%, we can calculate the ratio of the masses of the core and the shell, which, in the case $x = 1$, will be 35.2%. In the synthesis of $Cd_{0.25}Zn_{0.75}Se/ZnS$ (1–5 MLs) QDs, we took 0.196 g of the core (in terms of pure selenide 0.17 g):

$$v, \text{ mol (ZnS)} = \frac{0.17 \cdot 0.352}{M(\text{ZnS})} = \frac{0.06}{97.474} = 6.15 \cdot 10^{-4} \text{mol} = v, \text{ mol } (TU) \quad (4)$$

Using this approach, the amounts of (Z)-1-(octadec-9-enyl)-3-phenylthiourea (*TU*) taken to form 2, 3, 4, and 5 MLs were also calculated, respectively.

3.2. Morphology and Analytical Characterization of $Cd_{0.25}Zn_{0.75}Se/ZnS$ (1–5 MLs) QDs

Figure 2a displays X-ray patterns for $Cd_{0.25}Zn_{0.75}Se$ core/shell QDs with different thicknesses of the ZnS shell. The diffraction peaks for all samples lie between corresponding peaks for bulk cubic crystalline phases of $Cd_{0.2}Zn_{0.8}Se$ (ICSD 98-019-2340) and ZnS (ICSD 98-005-3943) (the respective XRD patterns are given at the bottom and top of Figure 2a). The whole series of prepared QDs have broadened peaks, which indicate small particle sizes. The X-ray diagram of the $Cd_{0.25}Zn_{0.75}Se$ core possesses a face-centered cubic structure with the space group $F\bar{4}3m$. The three prominent peaks at $2\theta = 26.5$, 44.3, and 52.2° are located between the respective peaks for bulk ZnSe (ICSD 98-016-7830) and CdSe (ICSD 98-018-7310), which suggests a successful formation of the alloyed crystal structure of $Cd_{0.25}Zn_{0.75}Se$ QDs. Reflection with the highest intensity observed from $Cd_{0.25}Zn_{0.75}Se$ QDs originated from the (111) crystallographic plane. No other peaks from Cd or Zn impurity phases were detected in the XRD patterns of $Cd_{0.25}Zn_{0.75}Se$ QDs. The presented data are consistent with our previous report [15].

During the overcoating process with the ZnS shell, the crystal structure of the $Cd_{0.25}Zn_{0.75}Se/ZnS$ QDs remains unchanged, i.e., zinc-blended crystalline structure. It is clearly visible that with an increase in the shell thickness, there is a gradual shift in the peak to larger 2θ angles, pointing to the formation of the ZnS-rich phase. Such shifts in the characteristic peaks further highlight the influence of the ZnS shell on the $Cd_{0.25}Zn_{0.75}Se/ZnS$ core/shell QDs and agree well with the results from TEM measurements and optical properties.

The presented X-ray diffraction results are well-matched with the literature [38]. The lattice parameters of the core (5.7934 Å) and shell (4.9510 Å) and mean particle size were calculated from the Scherrer equation [34].

Figure 2b,c show TEM and HRTEM images of as-prepared $Cd_{0.25}Zn_{0.75}Se$ QDs correspondingly. A dilute solution of QDs in chloroform was sonicated for 10 min and deposited on a TEM copper grid with an electron transparent membrane from graphene oxide. As can be seen from Figure 2b,c, the QDs were quite monodisperse and had a quasi-spherical shape. The interatomic distance in the core was 0.35 nm. Upon overcoating 1 and 2 MLs of ZnS shell on the surface of the $Cd_{0.25}Zn_{0.75}Se$ QDs core, epitaxial growth of the ZnS shell was observed (Figure 3a,b). Onwards, with a ZnS 3 ML overcoating, partially epitaxial growth was noticed (Figure 3c). Further growth of the ZnS shell to 5 MLs exhibited nonepitaxial growth, which was confirmed by HRTEM (Figure 4b,c).

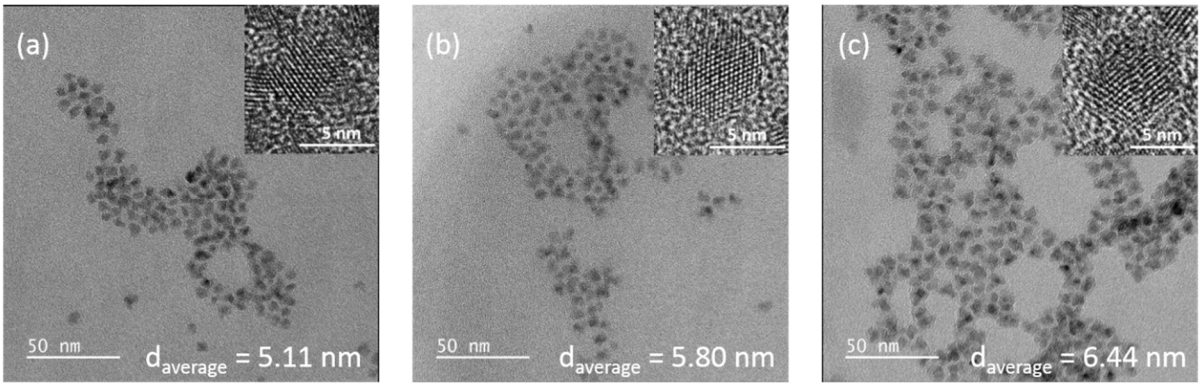

Figure 3. TEM and HRTEM (inset) images of $Cd_{0.25}Zn_{0.75}Se$/ZnS 1 ML (**a**), $Cd_{0.25}Zn_{0.75}Se$/ZnS 2 MLs (**b**), and $Cd_{0.25}Zn_{0.75}Se$/ZnS 3 MLs (**c**).

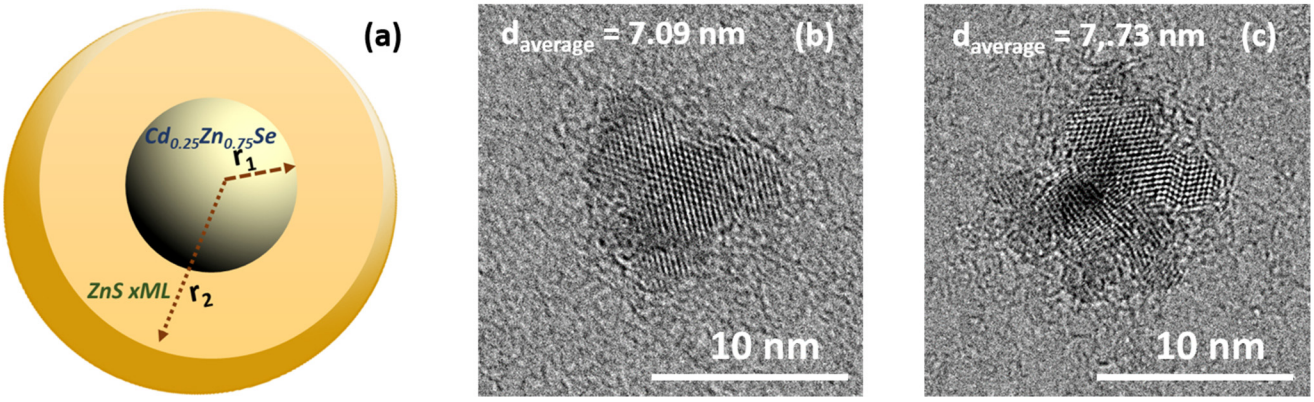

Figure 4. Theoretical model of core/shell quantum dot (**a**), HRTEM images of $Cd_{0.25}Zn_{0.75}Se$/ZnS 4 MLs (**b**), and $Cd_{0.25}Zn_{0.75}Se$/ZnS 5 MLs (**c**).

Figure 5 demonstrates HAADF-STEM imaging and corresponding energy dispersive X-ray spectroscopy (EDS) mapping for the core ($Cd_{0.25}Zn_{0.75}Se$) and for core/shell QDs ($Cd_{0.25}Zn_{0.75}Se$/ZnS 4 MLs). It can be seen from this figure that in the core, all elements (Cd, Zn, and Se) are present in the entire volume of the QD. At the same time, for $Cd_{0.25}Zn_{0.75}Se$/ZnS 4 ML QDs, the presence of Cd and Se is observed only in the core, while Zn and S are distributed in the entire volume of the QD. These results revealed that Cd, Zn, and Se are distributed homogeneously in QDs. There is no visual element aggregation or separation. The intensity of these signals is in good agreement with the nominal compositions of QDs.

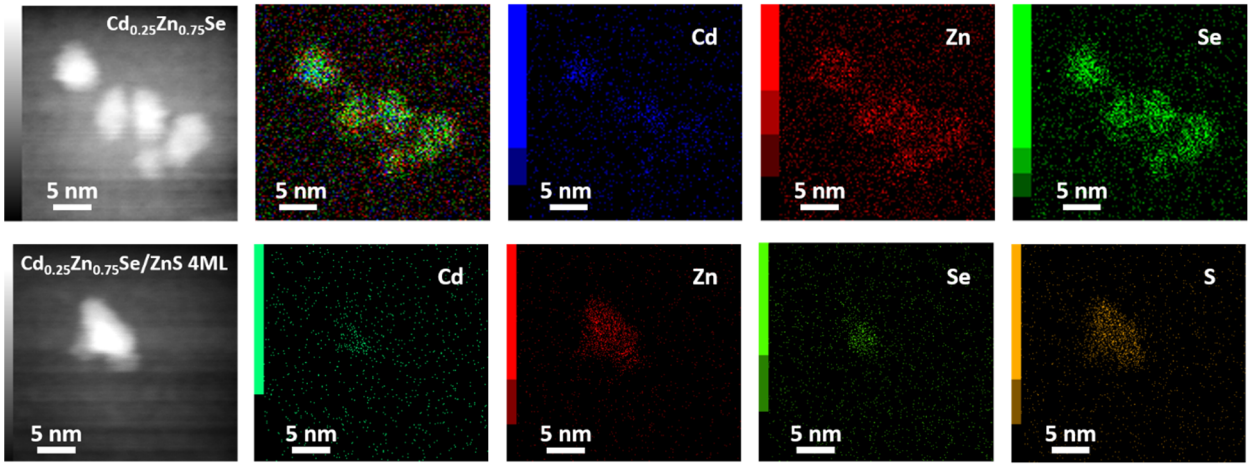

Figure 5. HAADF-STEM image and corresponding EDS elemental mapping of Cd, Zn, S, and Se of $Cd_{0.25}Zn_{0.75}Se/ZnS$ core/shell QDs.

The elemental analysis data of the QDs measured by the EDS and XPS analysis are summarized in Table 1. According to the data, the ratio of elements in the core material is consistent with the nominal composition. When the shell grows, the ratios of metals and chalcogens change according to the calculated amounts of substances taken into the synthesis. The ratios of the elements determined by XPS analysis differ from the nominal ones while corresponding to the QDs sizes. Signals corresponding to carbon and oxygen were also detected. These signals are attributed to metal linoleates present on the surface of the QDs as a protective shell. Traces of nitrogen, also found in the EDS spectrum, belong to the *co*-ligand oleylamine.

Table 1. Elemental composition of $Cd_{0.25}Zn_{0.75}Se/ZnS$ core/shell QDs measured by EDS * and XPS ** technique.

Composition	EDS				XPS			
	Cd, at.%	Zn, at.%	Se, at.%	S, at.%	Cd, at.%	Zn, at.%	Se, at.%	S, at.%
$Cd_{0.25}Zn_{0.75}Se$	14.7	41.2	44.1	-	16.3	48.2	35.6	-
$Cd_{0.25}Zn_{0.75}Se/ZnS$ 1 ML	7.4	48.1	23.6	20.9	7.5	53.4	15.5	23.7
$Cd_{0.25}Zn_{0.75}Se/ZnS$ 2 MLs	5.8	48.5	15.9	29.8	4.3	54.5	10.4	30.9
$Cd_{0.25}Zn_{0.75}Se/ZnS$ 3 MLs	3.5	51.2	11.1	34.2	2.4	55.2	6.1	36.8
$Cd_{0.25}Zn_{0.75}Se/ZnS$ 4 MLs	2.5	52.3	8.1	37.1	1.6	55.9	4.0	38.5
$Cd_{0.25}Zn_{0.75}Se/ZnS$ 5 MLs	2.1	52.7	6.6	38.6	1.2	55.6	3.6	39.7

* Theoretical error value for EDS is 1% ** Theoretical error value for XPS is 0.1%.

The surface chemical state of $Cd_{0.25}Zn_{0.75}Se/ZnS$ QDs was studied by XPS. The presence of C, O, Cd, Zn, Se, and S was confirmed through the survey spectra displayed in Figure 6a. Carbon and oxygen signals are due to the organic ligands from the precursors. Cd, Zn, and Se peaks correspond to the core of QDs; however, Zn is also part of the shell, as well as sulfur. In addition, the change in intensity of the Zn signal of the core sample with respect to the core/shell samples was observed. This was due to the fact that by adding the ZnS, a greater amount of zinc would be detected. This effect is more visible with sulfur and selenium, as the sulfur signal (S *2p*) increases as more ZnS is added in the QDs, and the selenium signal (Se *3d*) consequently decreases, as presented in Figure 6b. Additionally, Table 1 displays the results of the elemental composition of the samples and it demonstrates the aforementioned trend.

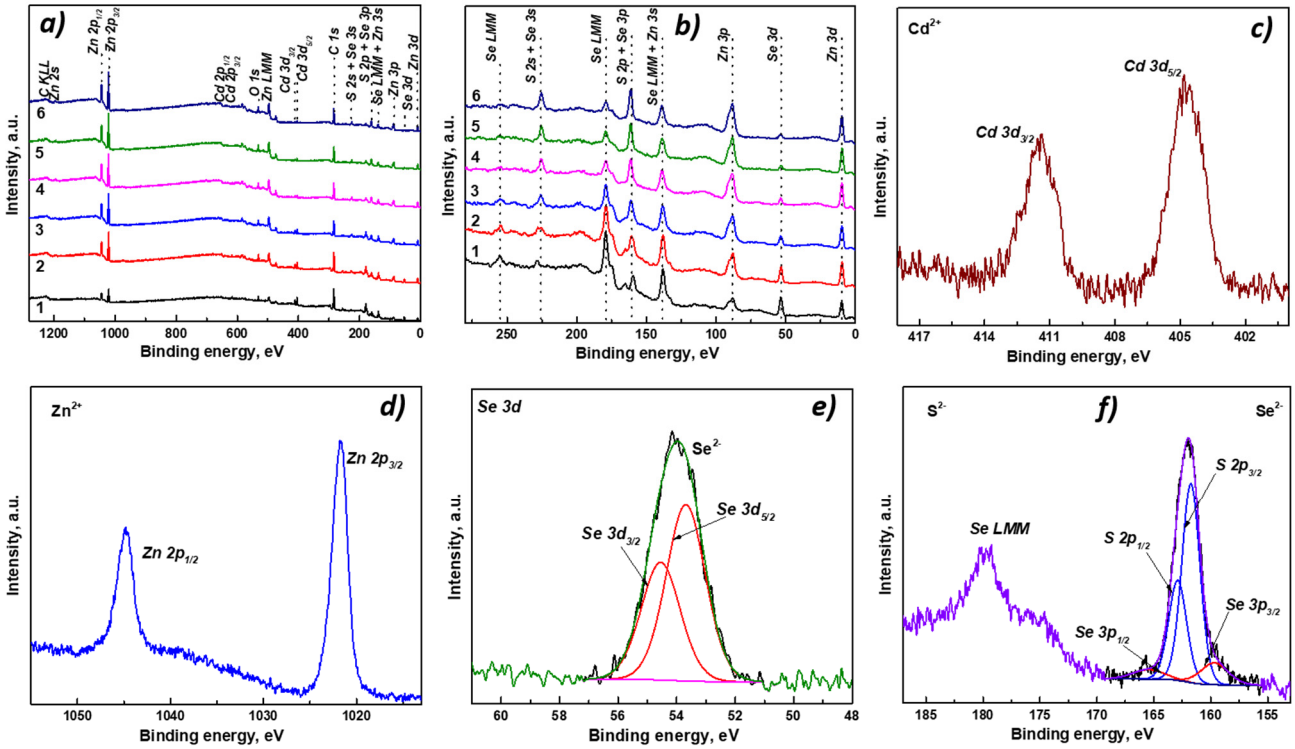

Figure 6. XPS survey spectra of core/shell $Cd_{0.25}Zn_{0.75}Se$/ZnS QDs with different shell thicknesses (1—$Cd_{0.25}Zn_{0.75}Se$ core, 2—ZnS 1 ML, 3—ZnS 2 MLs, 4—ZnS 3 MLs, 5—ZnS 4 MLs, 6—ZnS 5 MLs) (**a**,**b**); chemical state analysis of Cd *3d* (**c**), Zn *2p* (**d**), and Se *3d* (**e**), and strong overlap between S *2p* and Se *3p* (**f**).

Figure 6c displays the Cd 3*d* high-resolution (HR) spectrum of core/shell QDs, where its spin–orbit splitting Cd $3d_{5/2}$/Cd $3d_{3/2}$ signals are centered at ~404.8 eV/411.5 eV, assigned to the Cd^{2+} state related to Cd-Se bonds [39,40]. The Zn 2*p* HR spectrum is illustrated in Figure 6d, and its doublet, Zn $2p_{3/2}$/Zn $2p_{1/2}$, appears at ~1021.8 eV/ 1044.8 eV and suggests the presence of Zn^{2+} [41,42]. In the Se 3*d* HR spectrum displayed in Figure 6e, the presence of Se^{2-} species was found, as the spin–orbit signal Se $3d_{5/2}$/Se $3d_{3/2}$ is located at ~53.8 eV/54.7 eV [39,40]. In Figure 6f, a strong overlap between the S 2*p* and Se 3*p* signals is evidenced. The spectrum was deconvoluted with four components, and the most intense pair corresponds to the spin–orbit splitting of sulfur S $2p_{3/2}$/S $2p_{1/2}$, centered at ~161.7 eV/162. 9 eV, which is attributed to S^{2-} species, related to the Zn-S bond from the shell [42,43]. The less intense doublet Se $3p_{3/2}$/Se $3p_{1/2}$ located at ~160.2 eV/166.0 eV confirms the presence of Se^{2-} found in Se 3*d* signal [39].

The Raman spectra of $Cd_{0.25}Zn_{0.75}Se$/ZnS core/shell QDs series with different shell thicknesses are presented in Figure 7a. In the case of the core $Cd_{0.25}Zn_{0.75}Se$ sample, the only dominant band with maxima 248 cm^{-1} can be observed in the Raman spectra. This band can be attributed to longitudinal optical (LO) phonons in cubic $Cd_{0.25}Zn_{0.75}Se$ QDs [44,45]. When the core is encased within a ZnS shell, the new peaks attributed to the shell appear. The intensity of the band at 248 cm^{-1} gradually decreases with the growing thickness of the ZnS shell, and for the $Cd_{0.25}Zn_{0.75}Se$/ZnS (5 MLs) QDs, only a very weak shoulder is visible. The new bands at 218 cm^{-1}, 273 cm^{-1}, and 339 cm^{-1} are associated with longitudinal acoustical (LA) overtones and transverse optical (TO) and longitudinal optical (LO) phonon modes, and the less intense bands at 406 cm^{-1} and 425 cm^{-1} can be assigned to the sum (TO + LA) and (LO + TA) combination bands [35,46]. These results are good confirmation of the gradual growth of ZnS layers around the $Cd_{0.25}Zn_{0.75}Se$ core.

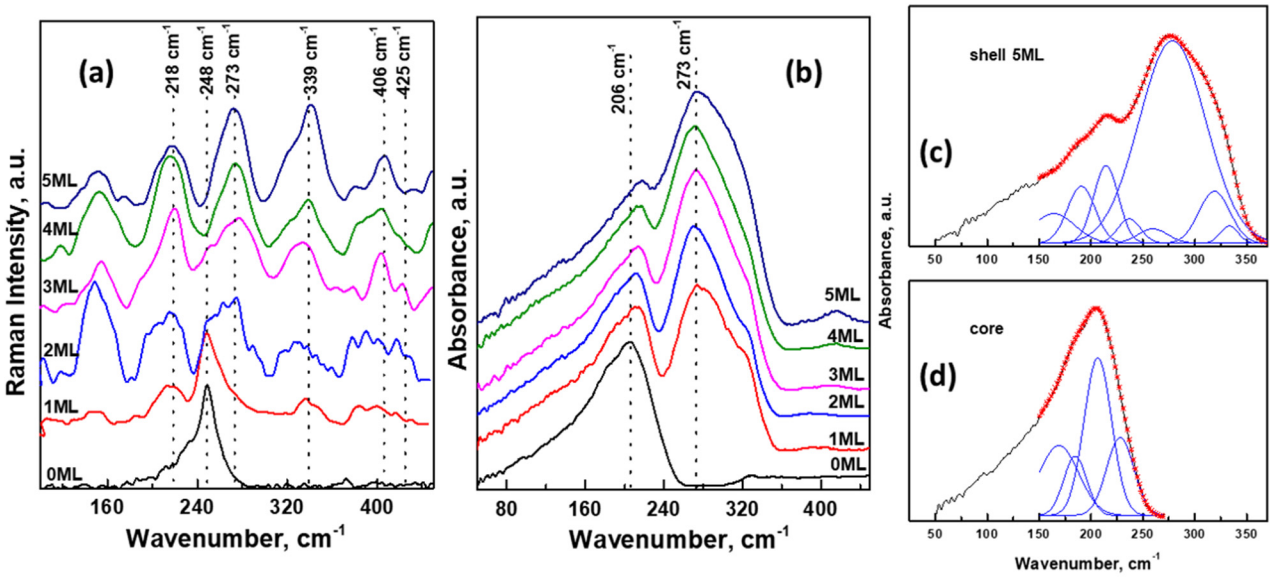

Figure 7. Raman (**a**) and ATR (**b**) spectra of $Cd_{0.25}Zn_{0.75}Se/ZnS$ (0–5 MLs) in the region 50–450 cm^{-1}; the decomposition of ATR spectra of $Cd_{0.25}Zn_{0.75}Se/ZnS$ (5 MLs) (**c**) and core (**d**).

ATR spectra of $Cd_{0.25}Zn_{0.75}Se/ZnS$ core/shell QDs in the region 50–450 cm^{-1} are demonstrated in Figure 7b. In this region, the main absorbance bands of inorganic nanoparticles are located. The ATR spectrum of pure $Cd_{0.25}Zn_{0.75}Se$ QDs contains a relatively strong band with maxima at 206 cm^{-1} in the spectral region of 50–250 cm^{-1}. The growth of the ZnS shell causes the appearance of a new intensive band with maxima at 273 cm^{-1} in the region between 230 cm^{-1} and 360 cm^{-1}. The intensity of this band enhances with increasing layer thickness, while the intensity of the first band (at 206 cm^{-1}) remains the same. ATR spectra were deconvoluted into several separate individual bands (as an example, decomposed spectra of core $Cd_{0.25}Zn_{0.75}Se$ and $Cd_{0.25}Zn_{0.75}Se/ZnS$ (5 MLs) QDs are illustrated in Figure 7c,d). The intensity of absorbance bands in the region of lower wavenumbers was influenced by the background due to the lower sensitivity of the detector and ATR crystal in this area; therefore, the figures display deconvolutions only in the area of the main vibration bands (150–370 cm^{-1}). In the case of pure $Cd_{0.25}Zn_{0.75}Se$ QDs (Figure 7d), the spectra were decomposed into four bands: strong band at 206 cm^{-1} and medium bands at 168 cm^{-1}, 184 cm^{-1}, and 225 cm^{-1}. These frequencies are in good agreement with the frequencies of vibration modes obtained from the reflection spectra of $Cd_xZn_{1-x}Se$ alloys [47]. The strongest band can be assigned to TO vibrations in $Cd_{0.25}Zn_{0.75}Se$ QDs. In the case of core/shell samples (Figure 7c), the spectra were decomposed into 8 bands. Likely, the first four bands are again related to vibrations in the $Cd_{0.25}Zn_{0.75}Se$ core. The second four bands at 259 cm^{-1}, 278 cm^{-1}, 318 cm^{-1}, and 333 cm^{-1} can be assigned to vibrations in the ZnS shell with cubic structure [48,49]. These results are in good agreement with those obtained from the Raman spectra of our samples.

3.3. Optical Properties of $Cd_{0.25}Zn_{0.75}Se/ZnS$ (1–5 MLs) QDs

One of the main goals of coating QDs with a thin layer of nanomaterial with different compositions is to change their optical characteristics. It is known that with the appropriate selection of the shell material, it is possible to achieve a manifold rise in the PL quantum yield and/or desired wavelength shift [50]. In the study of optical properties of the synthesized core/shell $Cd_{0.25}Zn_{0.75}Se/ZnS$ (0–5 MLs) QDs, it was found that a change in the excitation wavelength affects only the intensity of the emission signal, without any variations in their form and position. The given tendency persists for each of the studied samples. Therefore, for the assessment and comparative analysis of emission signals, solutions of $Cd_{0.25}Zn_{0.75}Se/ZnS$ (0–5 MLs) QDs were excited by light at λ_{max} so the intensity of the emission signal was maximum. Thus, the ratio of the intensities of the

main and additional photoluminescence emission peaks was retained for all core/shell $Cd_{0.25}Zn_{0.75}Se/ZnS$ QDs. Figure 8 displays the absorbance (black curves), excitation (blue), and emission (dark green) spectra of $Cd_{0.25}Zn_{0.75}Se/ZnS$ (1–5 MLs) QDs. As follows from Figure 8, an increase in the number of ZnS monolayers in the $Cd_{0.25}Zn_{0.75}Se$ QDs shell affected the spectra of all abovementioned characteristics.

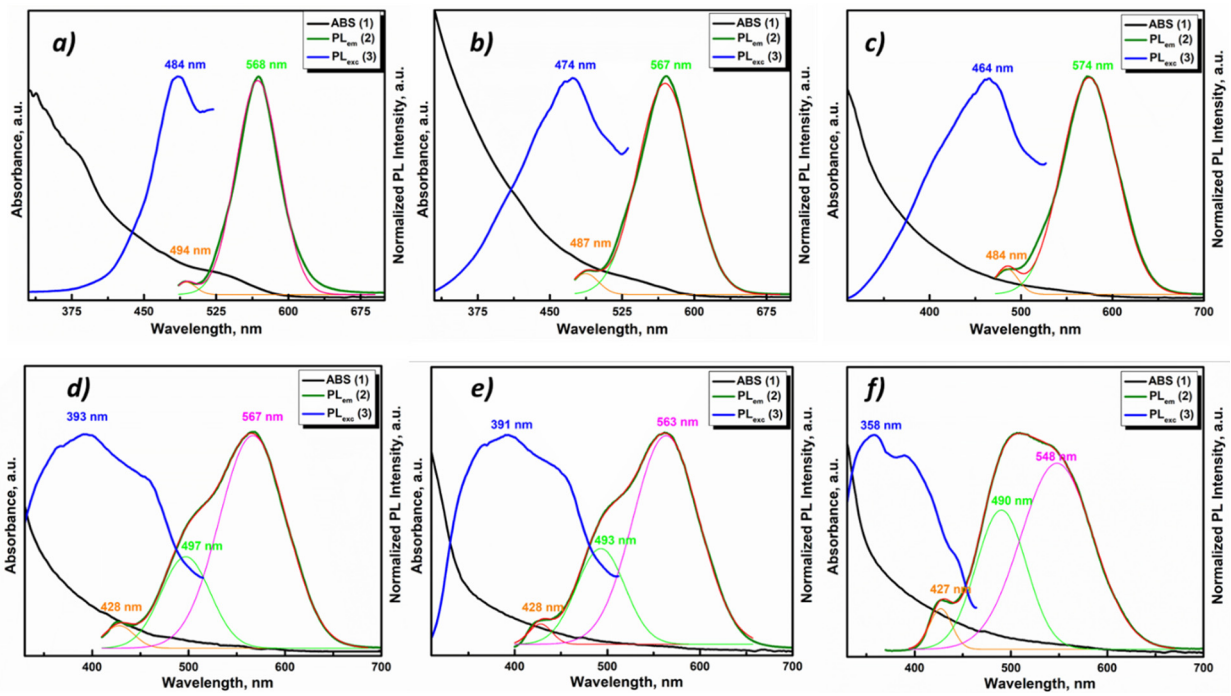

Figure 8. Normalized ABS, PL excitation, and PL emission spectra of core/shell $Cd_{0.25}Zn_{0.75}Se/ZnS$ QDs with different shell thicknesses: (**a**) $Cd_{0.25}Zn_{0.75}Se$ core, (**b**) ZnS 1 ML, (**c**) ZnS 2 MLs, (**d**) ZnS 3 MLs, (**e**) ZnS 4 MLs, and (**f**) ZnS 5 MLs.

In the absorbance (ABS) spectrum of $Cd_{0.25}Zn_{0.75}Se$ QDs, there is a weak peak in the region of 530–540 nm (Figure 8a), which is caused by the absorbance of an exciton. At the moment of the ZnS shell increment in the $Cd_{0.25}Zn_{0.75}Se$ core, this peak smooths out (1 ML ZnS Figure 8b), and after, completely disappears from the ABS spectra of $Cd_{0.25}Zn_{0.75}Se/ZnS$ QDs (2–5 MLs) QDs (Figure 8c–f). It can be caused by a growing size of $Cd_{0.25}Zn_{0.75}Se/ZnS$ QDs (1–5 MLs) QDs, as the exciton intensity decreases with the QD's size. Coating $Cd_{0.25}Zn_{0.75}Se$ QDs with ZnS 1 ML enlarges the size of QDs by ≈0.6 nm in diameter, which is 13% for $Cd_{0.25}Zn_{0.75}Se$ QDs 4.54 nm in size. In addition, the band gap values of $Cd_{0.25}Zn_{0.75}Se/ZnS$ QDs (1–5 MLs) were estimated from the absorbance spectra using the Tauc equation [51]. The calculation results are presented in Table 2.

Table 2. Optical properties of core/shell $Cd_{0.25}Zn_{0.75}Se/ZnS$ QDs and parameters of PL decay curves evaluation. Peak maximum in the PLE spectra (λ_{exc}), peak maximum in the PL spectra (λ_{em}), Stokes shift and band gap (E_g); fitting results: time constants τ_1, τ_2, τ_3; amplitude components A_1, A_2 and A_3; average lifetime τ_{avg}.

Number of Monolayers	Optical Parameters				Fitting Results of the PL Decay Curves						
	λ_{exc}, nm	λ_{em}, nm	QY,%	E_g, eV	τ_1, ns	τ_2, ns	τ_3, ns	A_1	A_1	A_1	τ_{avg}, ns
0	484	569	54	2.96	1.3	11.4	44.4	0.72	0.25	0.03	4.95
1	474	571	72	3.59	1.4	11.0	26.8	0.42	0.45	0.13	9.11
2	464	574	83	3.58	1.6	11.6	30.3	0.46	0.40	0.14	9.56
3	393	568	78	3.08	2.1	14.1	69.9	0.64	0.34	0.02	7.31
4	391	563	64	3.69	1.9	13.8	63.3	0.67	0.32	0.01	6.61
5	358	507	57	3.55	1.7	13.1	86.1	0.71	0.28	0.01	5.80

Following the increase in the number of monolayers on the surface of the core, significant changes in the PL excitation and emission spectra can be seen. For a more informative presentation, the emission spectra were decomposed into Gaussians. The excitation and emission spectra of the $Cd_{0.25}Zn_{0.75}Se$ core are represented by narrow Gaussian bands (Figure 8a). A small, low-intensity peak in the blue region of the spectrum can be caused by scattering and reabsorption of the sample photoluminescence due to the high excitation density. When ZnS 1 (Figure 8b) and 2 MLs (Figure 8c) were incremented to the $Cd_{0.25}Zn_{0.75}Se$ core, the PL excitation spectra noticeably broadened, and their maximum shifted to the blue region (see Table 2). In addition, there is some broadening in the emission spectra with a shift in the maxima toward the red region of the spectrum (λ_{em} = 567 nm and λ_{em} = 574 nm for $Cd_{0.25}Zn_{0.75}Se/ZnS$ QDs 1 ML and 2 MLs, respectively). When the ZnS 1 ML grows on the $Cd_{0.25}Zn_{0.75}Se$ core, PL QY rises from 54% (for the $Cd_{0.25}Zn_{0.75}Se$ core) to 83% (for the $Cd_{0.25}Zn_{0.75}Se/ZnS$ 2 MLs) (Figure 9a). With a subsequent augmentation of the shell thickness to 3–5 MLs, additional components appear in the PL excitation and emission spectra, and their maxima shift toward the high-energy spectral region. In addition, with an increase in the number of ZnS MLs, the intensity of the main PL component (λ_{em} = 567 nm, 563 nm, and 548 nm for $Cd_{0.25}Zn_{0.75}Se/ZnS$ 3 ML, 4 ML, and 5 ML QDs, respectively) decreases, while the additional PL component that appears (λ_{em} = 497 nm, 493 nm, and 490 nm for $Cd_{0.25}Zn_{0.75}Se/ZnS$ 3 ML, 4 ML, and 5 ML QDs, respectively) becomes dominant (Figure 8d–f). An increase in the thickness of the $Cd_{0.25}Zn_{0.75}Se/ZnS$ QDs shell from 3 MLs and more has a strong effect on the PL intensity. For $Cd_{0.25}Zn_{0.75}Se/ZnS$ 3 ML QDs, the PL QY decreases to 78%, and with subsequent growth in the number of ZnS MLs up to 5, the PL QY drops to 57% (Figure 9a). Such changes in the PL spectra of $Cd_{0.25}Zn_{0.75}Se/ZnS$ QDs with rising shell thickness were caused by a change in the parameters of its growth on the surface of the $Cd_{0.25}Zn_{0.75}Se$ core. On TEM images (Figure 3a,b), it was clearly visible that with increment in the ZnS 1 and 2 MLs to the $Cd_{0.25}Zn_{0.75}Se$ core, the shell grows epitaxially. This means that the first two ZnS MLs grow evenly distributed over the surface of the core, "healing" most of the surface defects. This "healing" of defects leads to an increase in the PL intensity, almost without affecting the shape of the spectrum. The growth in the 4 or 5 MLs no longer occurs epitaxially to the core (Figure 4b,c). As the layer thickness is comparable with the crystal lattice parameter, and the further growing ZnS layer no longer interacts with the core, a ZnS monolayer increments on the surface with a lot of defects [50,52]. Increasing the shell thickness also leads to an enhancement in the volume/mass ratio of the shell and core. As can be seen from Figure 8d, an additional component (λ_{em} = 497 nm) appears in the PL spectrum of $Cd_{0.25}Zn_{0.75}Se/ZnS$ 3 ML QDs, which is induced by the luminescence of the shell. Consequently, the shell no longer amplifies the PL of the core, but already has its own PL, which means that it will absorb the exciting light.

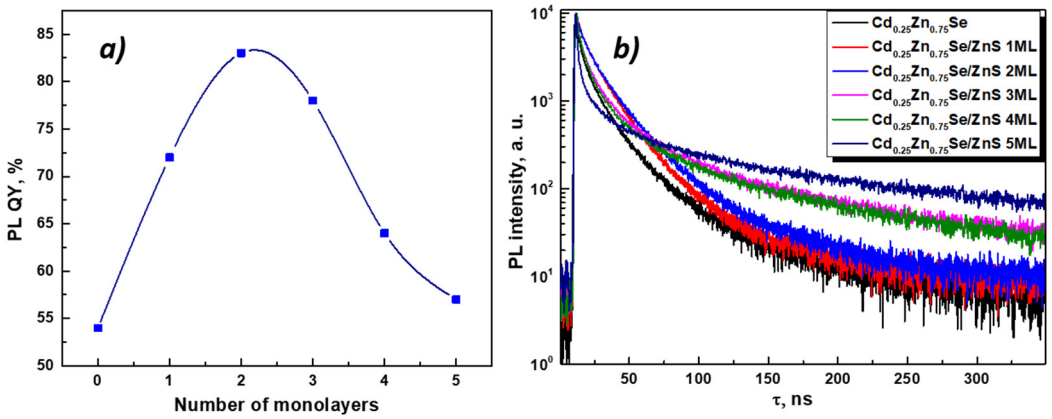

Figure 9. PL QY dependence on the shell thickness (**a**) and PL decay kinetic curves (**b**) of core/shell $Cd_{0.25}Zn_{0.75}Se/ZnS$ QDs.

As mentioned above, the number of surface defects decreases with epitaxial growth and increases with nonepitaxial growth. To confirm this statement, the quenching PL kinetics curves of core/shell $Cd_{0.25}Zn_{0.75}Se/ZnS$ QDs were measured (Figure 9b). The quenching kinetics of a single crystal without defects consists of one exponential component. However, the surface of nanocrystals is characterized by many nonpassivated states (defects), which provide additional (radiative and nonradiative) relaxation paths of charge carriers. Due to that, the PL quenching kinetics of nanosized crystals is multi-exponential [53]. A change in the number of surface defects leads to a change in the PL quenching kinetics curves. The quenching kinetics curves measured for PL core/shell $Cd_{0.25}Zn_{0.75}Se/ZnS$ QDs are multi-exponential. They were fitted using Equation (5):

$$I(t) = \int_0^t IRF(t') \left(C + \sum_{i=1}^{3} A_i \exp\left(-\frac{t - t'}{\tau_i} \right) \right) dt' \quad (5)$$

where *IRF* is the instrument response function, and τ_i and A_i are the PL decay time and amplitudes components, respectively. The average lifetime is calculated using Equation (6):

$$\tau_{avg} = \frac{\sum_{i=1}^{3} A_i \tau_i}{\sum_{i=1}^{3} A_i} \quad (6)$$

As follows from Figure 9b, when the ZnS 1 and 2 MLs were deposited onto the $Cd_{0.25}Zn_{0.75}Se$ core, the quenching kinetics curves were slightly aligned (red and blue curves, respectively). This was also confirmed by the fitting results of the PL quenching kinetic curves of core/shell $Cd_{0.25}Zn_{0.75}Se/ZnS$ QDs presented in Table 2. When the $Cd_{0.25}Zn_{0.75}Se$ core is covered with one or two ZnS MLs, the component with $\tau \approx 11$ ns becomes dominant. At the same time, for the $Cd_{0.25}Zn_{0.75}Se$ core, the main contribution is made by the fastest component (τ = 1.3 ns). According to other authors, the exciton lifetime in CdZnSe is in the range of 7–15 ns [3,54]. The presence of a fast PL quenching component is caused by the interaction of an exciton with energetically deep surface defects and its nonradiative relaxation [53]. Reducing the contribution of this component indicates a decrease in the number of defects and, as a result, an enhancement in the PL intensity. With the growth in the shell thickness to ZnS 3 MLs, the main contribution is again made by the fast component. It should also be noted that further growth in the number of ZnS MLs leads to a reduction in this component and a significant increase in its contribution (τ = 2.1 ns and A = 64%, and τ = 1.7 ns and A = 71% for ZnS 3 and 5 MLs, respectively). Last but not least, with a shell growth from ZnS 3 MLs, the last and slowest time component of the quenching kinetics of core/shell $Cd_{0.25}Zn_{0.75}Se/ZnS$ QDs rises from τ = 30.3 ns for ZnS 2 MLs to τ = 69.9 ns for ZnS 3 MLs and τ = 86.1 ns for ZnS 5 MLs. The gain of the slow component indicates an augmentation in the interaction of charge carriers with small surface defects [53]. From the above, it follows that the growth of the ZnS shell thickness for $Cd_{0.25}Zn_{0.75}Se/ZnS$ QDs by more than two monolayers leads to negative consequences, namely, an increase in the number of surface defects and a decrease in the PL core/shell $Cd_{0.25}Zn_{0.75}Se/ZnS$ QDs intensity.

4. Conclusions

To conclude, we have presented the employment of an efficient and highly controlled methodology for growing the binary ZnS shell on ternary $Cd_{0.25}Zn_{0.75}Se$ quasi-spherical QDs, which can be prepared on a multigram scale (e.g., 3.5 g per one batch). The method is based on the calculated volume and mass ratios of the core to the shell. This calculation allowed us to minimize the required materials to the shell growth of a desired thickness without the formation of independent ZnS crystals. It has also been demonstrated that substituted selenourea (i.e., (*Z*)-*N*-(octadec-9-enyl)morpholine-4-carboselenoamide), taken as a new source of selenium, was successfully combined with the already presented substituted thiourea (i.e., (*Z*)-1-(octadec-9-enyl)-3-phenylthiourea) within the synthesis of

core/shell $Cd_{0.25}Zn_{0.75}Se$/ZnS QDs. Raman and FT-IR spectral studies, as well as EDS and XPS analysis of the core/shell $Cd_{0.25}Zn_{0.75}Se$/ZnS QDs, confirmed full accordance with the declared compositions. According to the TEM and optical studies, the 1 and 2 ML shells grew epitaxially to the core, the 3 ML shell grew partially epitaxially to the core, and a further increment in ZnS was characterized by nonepitaxial shell growth. Investigation of the PL properties of core/shell $Cd_{0.25}Zn_{0.75}Se$/ZnS 1–5 ML QDs revealed the PL QY considerable magnification (up to 83%) with the increment of 1 and 2 MLs of ZnS, which indicates the inhibition of nanocrystal's surface defects. With a further shell thickness rise, new defects appeared, which led to a decrease in the PL QY. According to the experimental data, the 2 ML ZnS shell is optimal from the point of view of the morphology and optical properties of this nanomaterial. The method presented here certainly contributes to the development of further research and, due to its simplicity and accuracy, can be transferred to an industrial scale.

Author Contributions: Conceptualization and methodology, L.L.; XRD, PL, and lifetime measurements, M.C. (Maksym Chylii); STEM survey measurements and EDS measurements, S.S.; NMR measurements, P.S.; XPS measurements, J.R.P.; Raman and FT-IR measurements, B.F.; TEM, HR TEM, and STEM/EDS mapping measurements, M.C. (Miroslav Cieslar); formal analysis, A.K.; investigation, L.L.; writing—original draft preparation, L.L., M.C. (Maksym Chylii), A.K., J.R.P. and B.F.; writing—review and editing, all authors; supervision, M.V.; project administration, M.V. All authors have read and agreed to the published version of the manuscript.

Funding: This research was funded by the Ministry of Education, Youth and Sports of the Czech Republic, projects numbers "High-sensitive and low-density materials based on polymeric nanocomposites"—NANOMAT (No. CZ.02.1.01/0.0/0.0/17_048/0007376) and grant LM2018103.

Institutional Review Board Statement: Not applicable.

Informed Consent Statement: Not applicable.

Conflicts of Interest: The authors declare no conflict of interest.

References

1. Alivisatos, A.P. Semiconductor Clusters, Nanocrystals, and Quantum Dots. *Science* **1996**, *271*, 933–937. [CrossRef]
2. Pietryga, J.M.; Park, Y.-S.; Lim, J.; Fidler, A.F.; Bae, W.K.; Brovelli, S.; Klimov, V.I. Spectroscopic and Device Aspects of Nanocrystal Quantum Dots. *Chem. Rev.* **2016**, *116*, 10513–10622. [CrossRef]
3. Rabouw, F.T.; de Mello Donega, C. Excited-State Dynamics in Colloidal Semiconductor Nanocrystals. *Top. Curr. Chem.* **2016**, *374*, 58. [CrossRef] [PubMed]
4. Han, C.-Y.; Yang, H. Development of Colloidal Quantum Dots for Electrically Driven Light-Emitting Devices. *J. Korean Ceram. Soc.* **2017**, *54*, 449–469. [CrossRef]
5. Chandrasekhar, S.; Martinuzzi, S.; Nataren, F.Z. Improved efficiency of CdZnS thin-film solar cells. *Can. J. Phys.* **1985**, *63*, 716–718. [CrossRef]
6. Cao, D.; Yang, G. Quantum dot/polymer nanocomposite monolith for radiation detection. *Mater. Today Commun.* **2020**, *24*, 101246. [CrossRef]
7. Liu, C.; Li, Z.; Hajagos, T.J.; Kishpaugh, D.; Chen, D.Y.; Pei, Q. Transparent Ultra-High-Loading Quantum Dot/Polymer Nanocomposite Monolith for Gamma Scintillation. *ACS Nano* **2017**, *11*, 6422–6430. [CrossRef] [PubMed]
8. Brown, S.S.; Rondinone, A.J.; Pawel, M.D.; Dai, S. Ternary Cadmium Sulphide Selenide Quantum Dots as New Scintillation Materials. *Mater. Technol.* **2008**, *23*, 94–99. [CrossRef]
9. Huang, W.; Ge, S.; Lei, Y.; Zheng, Z. Composition-dependent perfect band gap tuning of ZnS_{1-x} Sex solid solutions for efficient photocatalysis. *J. Phys. Chem. Solids* **2019**, *130*, 41–45. [CrossRef]
10. Eskandari, P.; Kazemi, F.; Zand, Z. Photocatalytic reduction of aromatic nitro compounds using CdS nanostructure under blue LED irradiation. *J. Photochem. Photobiol. A Chem.* **2014**, *274*, 7–12. [CrossRef]
11. Bernt, C.M.; Burks, P.T.; DeMartino, A.W.; Pierri, A.E.; Levy, E.S.; Zigler, D.F.; Ford, P.C. Photocatalytic Carbon Disulfide Production via Charge Transfer Quenching of Quantum Dots. *J. Am. Chem. Soc.* **2014**, *136*, 2192–2195. [CrossRef] [PubMed]
12. Yong, K.T.; Roy, I.; Ding, H.; Bergey, E.J.; Prasad, P.N. Biocompatible Near-Infrared Quantum Dots as Ultrasensitive Probes for Long-Term in Vivo Imaging Applications. *Small* **2009**, *5*, 1997–2004. [CrossRef] [PubMed]
13. Zhong, X.; Feng, Y.; Zhang, Y.; Gu, Z.; Zou, L. A Facile Route to Violet- to Orange-Emitting $Cd_xZn_{1-x}Se$ Alloy Nanocrystals via Cation Exchange Reaction. *Nanotechnology* **2007**, *18*, 385606. [CrossRef]
14. Liu, F.-C.; Cheng, T.-L.; Shen, C.-C.; Tseng, W.-L.; Chiang, M.Y. Synthesis of Cysteine-Capped $Zn_xCd_{1-x}Se$ Alloyed Quantum Dots Emitting in the Blue−Green Spectral Range. *Langmuir* **2008**, *24*, 2162–2167. [CrossRef]

15. Loghina, L.; Iakovleva, A.; Chylii, M.; Svec, P.; Houdek, J.; Slang, S.; Palka, K.; Michalicka, J.; Vlcek, M. Synthetic Development in Cd–Zn–Se Quantum Dots Chemistry. *Opt. Mater.* **2019**, *97*, 109385. [CrossRef]
16. Shang, Y.; Ning, Z. Colloidal Quantum-Dots Surface and Device Structure Engineering for High-Performance Light-Emitting Diodes. *Natl. Sci. Rev.* **2017**, *4*, 170–183. [CrossRef]
17. Xu, S.; Shen, H.; Zhou, C.; Yuan, H.; Liu, C.; Wang, H.; Ma, L.; Li, L.S. Effect of Shell Thickness on the Optical Properties in CdSe/CdS/$Zn_{0.5}Cd_{0.5}$S/ZnS and CdSe/CdS/Zn_xCd_{1-X}S/ZnS Core/Multishell Nanocrystals. *J. Phys. Chem. C* **2011**, *115*, 20876–20881. [CrossRef]
18. Xie, H.Y.; Liang, J.G.; Liu, Y.; Zhang, Z.L.; Pang, D.W.; He, Z.K.; Lu, Z.X.; Huang, W.H. Preparation and Characterization of Overcoated II-VI Quantum Dots. *J. Nanosci. Nanotechnol.* **2005**, *5*, 880–886. [CrossRef]
19. Chaudhuri, R.G.; Paria, S. Core/Shell Nanoparticles: Classes, Properties, Synthesis Mechanisms, Characterization, and Applications. *Chem. Rev.* **2011**, *112*, 2373–2433. [CrossRef]
20. Huang, C.-H.; Yang, C.-H.; Shieh, Y.-T.; Wang, T.-L. Synthesis and Properties of Alloyed $Cd_xZn_{1-x}Se$ Core and Manganese-Doped $Cd_xZn_{1-x}Se$/ZnS Core/Shell Nanocrystals. *J. Alloys Compd.* **2018**, *748*, 265–272. [CrossRef]
21. Yang, H.; Holloway, P.H. Enhanced Photoluminescence from CdS:Mn/ZnS Core/Shell Quantum Dots. *Appl. Phys. Lett.* **2003**, *82*, 1965–1967. [CrossRef]
22. Qin, W.; Shah, R.A.; Guyot-Sionnest, P. CdSeS/ZnS Alloyed Nanocrystal Lifetime and Blinking Studies under Electrochemical Control. *ACS Nano* **2012**, *6*, 912–918. [CrossRef]
23. Rana, M.; Jain, A.; Rani, V.; Chowdhury, P. Glutathione Capped Core/Shell CdSeS/ZnS Quantum Dots as a Medical Imaging Tool for Cancer Cells. *Inorg. Chem. Commun.* **2020**, *112*, 107723. [CrossRef]
24. Jin, X.; Xie, K.; Zhang, T.; Lian, H.; Zhang, Z.; Xu, B.; Li, D.; Li, Q. Cation Exchange Assisted Synthesis of ZnCdSe/ZnSe Quantum Dots with Narrow Emission Line Widths and near-Unity Photoluminescence Quantum Yields. *Chem. Commun.* **2020**, *56*, 6130–6133. [CrossRef]
25. Li, Z.; Chen, F.; Wang, L.; Shen, H.; Guo, L.; Kuang, Y.; Wang, H.; Li, N.; Li, L.S. Synthesis and Evaluation of Ideal Core/Shell Quantum Dots with Precisely Controlled Shell Growth: Nonblinking, Single Photoluminescence Decay Channel, and Suppressed FRET. *Chem. Mater.* **2018**, *30*, 3668–3676. [CrossRef]
26. Zhang, T.; Zhang, X.; Yang, P.; Bai, J.; Chang, C.; Jin, X.; Zhao, F.; Huang, Y.; Li, F. Bright Alloy CdZnSe/ZnSe QDs with Nonquenching Photoluminescence at High Temperature and Their Application to Light-Emitting Diodes. *J. Nanomater.* **2019**, *2019*, 1–8. [CrossRef]
27. Hung, L.X.; Thang, P.N.; Van Nong, H.; Yen, N.H.; Chinh, V.Đ.; Van Vu, L.; Hien, N.T.T.; de Marcillac, W.D.; Hong, P.N.; Loan, N.T.; et al. Synthesis, Structural and Optical Characterization of CdTeSe/ZnSe and CdTeSe/ZnTe Core/Shell Ternary Quantum Dots for Potential Application in Solar Cells. *J. Electron. Mater.* **2016**, *45*, 4425–4431. [CrossRef]
28. Jiang, W.; Singhal, A.; Zheng, J.; Wang, C.; Chan, W.C.W. Optimizing the Synthesis of Red- to near-IR-Emitting CdS-Capped $CdTe_xSe_{1-x}$ Alloyed Quantum Dots for Biomedical Imaging. *Chem. Mater.* **2006**, *18*, 4845–4854. [CrossRef]
29. Xu, B.; Zhang, T.; Lin, X.; Yang, H.; Jin, X.; Huang, Z.; Zhang, Z.; Li, D.; Li, Q. One Pot Synthesis of Thick Shell Blue Emitting CdZnS/ZnS Quantum Dots with Narrow Emission Line Width. *Opt. Mater. Express* **2020**, *10*, 1232. [CrossRef]
30. Lee, Y.; Kim, S.; Kim, H.S.; Shin, J.B.; Choi, W.; Cho, H.; Kim, K.; Lee, T.; Kim, J.; Kang, I.B.; et al. Highly Luminescent Blue-Emitting CdZnS/ZnS Nanorods Having Electric-Field-Induced Fluorescence Switching Properties. *J. Mater. Chem. C* **2017**, *5*, 2098–2106. [CrossRef]
31. Fitzmorris, B.C.; Pu, Y.C.; Cooper, J.K.; Lin, Y.F.; Hsu, Y.J.; Li, Y.; Zhang, J.Z. Optical Properties and Exciton Dynamics of Alloyed Core/Shell/Shell $Cd_{1-x}Zn_xSe$/ZnSe/ZnS Quantum Dots. *ACS Appl. Mater. Interfaces* **2013**, *5*, 2893–2900. [CrossRef]
32. Zhang, Q.; Nie, C.; Chang, C.; Guo, C.; Jin, X.; Qin, Y.; Li, F.; Li, Q. Highly Luminescent Red Emitting CdZnSe/ZnSe Quantum Dots Synthesis and Application for Quantum Dot Light Emitting Diodes. *Opt. Mater. Express* **2017**, *7*, 3875. [CrossRef]
33. Susumu, K.; Field, L.D.; Oh, E.; Hunt, M.; Delehanty, J.B.; Palomo, V.; Dawson, P.E.; Huston, A.L.; Medintz, I.L. Purple-, Blue-, and Green-Emitting Multishell Alloyed Quantum Dots: Synthesis, Characterization, and Application for Ratiometric Extracellular PH Sensing. *Chem. Mater.* **2017**, *29*, 7330–7344. [CrossRef]
34. Iakovleva, A.; Loghina, L.; Zmrhalova, Z.O.; Mistrik, J.; Svec, P.; Slang, S.; Palka, K.; Vlcek, M. Environmentally friendly approach to the synthesis of monodisperse and bright blue emitting Cd0.15Zn0.85S quantum dots. *J. Alloy. Compd.* **2019**, *812*, 152159. [CrossRef]
35. Kaderavkova, A.; Loghina, L.; Chylii, M.; Slang, S.; Placek, P.; Frumarova, B.; Vlcek, M. N,N′,N′-Trisubstituted Thiourea as a Novel Sulfur Source for the Synthesis of Mn-Doped ZnS QDs. *J. Alloys Compd.* **2020**, *831*, 154814. [CrossRef]
36. Loghina, L.; Grinco, M.; Iakovleva, A.; Slang, S.; Palka, K.; Vlcek, M. Mechanistic Investigation of the Sulfur Precursor Evolution in the Synthesis of Highly Photoluminescent $Cd_{0.15}Zn_{0.85}S$ Quantum Dots. *New J. Chem.* **2018**, *42*, 14779–14788. [CrossRef]
37. Aharoni, A.; Mokari, T.; Popov, I.; Banin, U. Synthesis of InAs/CdSe/ZnSe Core/Shell1/Shell2 Structures with Bright and Stable Near-Infrared Fluorescence. *J. Am. Chem. Soc.* **2006**, *128*, 257–264. [CrossRef] [PubMed]
38. Shen, H.; Wang, S.; Wang, H.; Niu, J.; Qian, L.; Yang, Y.; Titov, A.; Hyvonen, J.; Zheng, Y.; Li, L.S. Highly Efficient Blue–Green Quantum Dot Light-Emitting Diodes Using Stable Low-Cadmium Quaternary-Alloy ZnCdSSe/ZnS Core/Shell Nanocrystals. *ACS Appl. Mater. Interfaces* **2013**, *5*, 4260–4265. [CrossRef] [PubMed]
39. Ospina, R.; Rincón-Ortiz, S.A.; Rodriguez-Pereira, J. Cadmium Selenide by XPS. *Surf. Sci. Spectra* **2020**, *27*, 014021. [CrossRef]

40. Liu, Y.; Dai, F.; Zhao, R.; Huai, X.; Han, J.; Wang, L. Aqueous Synthesis of Core/Shell/Shell CdSe/CdS/ZnS Quantum Dots for Photocatalytic Hydrogen Generation. *J. Mater. Sci.* **2019**, *54*, 8571–8580. [CrossRef]
41. Zimdars, J.; Pilger, J.; Entrup, M.; Deiting, D.; Schäfer, A.H.; Bredol, M. A Facile Synthesis of Alloyed Mn-Doped ZnSeS Nanoparticles Using a Modified Selenium/Sulfur Precursor in a One-Pot Approach. *New J. Chem.* **2016**, *40*, 8465–8470. [CrossRef]
42. Barreca, D.; Gasparotto, A.; Maragno, C.; Tondello, E.; Spalding, T.R. Analysis of Nanocrystalline ZnS Thin Films by XPS. *Surf. Sci. Spectra* **2002**, *9*, 54–61. [CrossRef]
43. La Porta, F.A.; Ferrer, M.M.; de Santana, Y.V.B.; Raubach, C.W.; Longo, V.M.; Sambrano, J.R.; Longo, E.; Andrés, J.; Li, M.S.; Varela, J.A. Synthesis of Wurtzite ZnS Nanoparticles Using the Microwave Assisted Solvothermal Method. *J. Alloy. Compd.* **2013**, *556*, 153–159. [CrossRef]
44. Alonso, R.G.; Suh, E.-K.; Ramdas, A.K.; Samarth, N.; Luo, H.; Furdyna, J.K. Raman Spectroscopy of Two Novel Semiconductors and Related Superlattices: Cubic Cubic $Cd_{1-x}Mn_xSe$ and $Cd_{1-x}Zn_xSe$. *Phys. Rev. B* **1989**, *40*, 3720–3728. [CrossRef] [PubMed]
45. Valakh, M.Y.; Lisitsa, M.P.; Pekar, G.S.; Polysskii, G.N.; Sidorenko, V.I.; Yaremko, A.M. Anharmonic Coupling of Phonon Modes in Mixed $Zn_xCd_{1-x}Se$ Crystals. *Phys. Status Solidi* **1982**, *113*, 635–645. [CrossRef]
46. Nilsen, W.G. Raman Spectrum of Cubic ZnS. *Phys. Rev.* **1969**, *182*, 838–850. [CrossRef]
47. Vodopyanov, L.K.; Vinogradov, E.A.; Vinogradov, V.S.; Kucherenko, I.V.; Mavrin, B.N.; Novikova, N.N.; Shapkin, P.V. Optical Phonons in $Zn_{1-x}Cd_xSe$ Alloys. *Phys. Status Solidi* **2004**, *1*, 3162–3165. [CrossRef]
48. Srivastava, S. Infrared Active Two-Phonon Processes in Cubic ZnS. *Aust. J. Phys.* **1973**, *26*, 111. [CrossRef]
49. Klein, C.A.; Donadio, R.N. Infrared-active Phonons in Cubic Zinc Sulfide. *J. Appl. Phys.* **1980**, *51*, 797–800. [CrossRef]
50. Yadav, A.N.; Singh, A.K.; Singh, K. Synthesis, Properties, and Applications of II–VI Semiconductor Core/Shell Quantum Dots. In *Core/Shell Quantum Dots*; Springer: Cham, Switzerland, 2020; pp. 1–28. [CrossRef]
51. Tauc, J.; Menth, A. States in the gap. *J. Non-Cryst. Solids* **1972**, *8–10*, 569–585. [CrossRef]
52. Gaikwad, A.P.; Tyagi, D.; Betty, C.A.; Sasikala, R. Photocatalytic and Photo Electrochemical Properties of Cadmium Zinc Sulfide Solid Solution in the Presence of Pt and RuS_2 Dual Co-Catalysts. *Appl. Catal. A Gen.* **2016**, *517*, 91–99. [CrossRef]
53. Wojtowicz, A.J.; Glodo, J.; Drozdowski, W.; Przegietka, K.R. Electron Traps and Scintillation Mechanism in $YAlO_3$:Ce and $LuAlO_3$:Ce Scintillators. *J. Lumin.* **1998**, *79*, 275–291. [CrossRef]
54. Morgan, D.P.; Kelley, D.F. Exciton Localization and Radiative Lifetimes in CdSe Nanoplatelets. *J. Phys. Chem. C* **2019**, *123*, 18665–18675. [CrossRef]